

Optimal control of circular cylinder wakes using long control horizons

Thibault L. B. Flinois^{*†} Tim Colonius[‡]

June 10, 2019

Abstract

The classical problem of minimizing the drag of a circular cylinder by using body rotation is revisited in an adjoint-based optimal control framework. The cylinder's unsteady and fully unconstrained rotation rate is optimized at Reynolds numbers of 100 and 200 and over horizons that are longer than in previous studies, where they are typically of the order of a vortex shedding period or shorter. In the best configuration, the drag is reduced by 19%, the vortex shedding is effectively suppressed, and this low drag state is maintained with minimal cylinder rotation after transients. Without closed-loop control, which maintains a specific phase relationship between the actuation and the shedding, the wake is not stabilized. A comparison is also given between the performance of optimizations for different horizon lengths and cost functions. It is shown that the long horizons used are necessary in order to stabilize the vortex shedding efficiently.

1 Introduction

The circular cylinder is often used to test and compare the ability of control methods to suppress flow instabilities. When the Reynolds number of the flow ($Re = U_\infty D/\nu$, where U_∞ is the inflow velocity, D is the cylinder diameter and ν is the kinematic viscosity) reaches about 47, the interaction between the two shear layers becomes linearly unstable, resulting in a supercritical Hopf bifurcation[30]. For higher Reynolds numbers, a stable limit cycle occurs in the form of the well-known Von Kármán vortex street, where vortices that are shed in turn from each side of the body.

When $47 \leq Re \leq 180$ the flow is unsteady and two-dimensional [39] and the suppression of the wake instability in this Reynolds number range has often been studied both for the simplicity of the cylinder geometry and for the industrial interest in reducing bluff-body form drag and wake fluctuations. A plethora of control methods have been applied to this setup and some of the most important and successful approaches were reviewed by Choi[10]. Usually, flow control strategies are categorized into passive methods, which do not require an energy input – such as splitter plates [3] or control cylinders [31, 34] – and active methods, which do – e.g. cross-flow body displacement [33], or cylinder rotation [37].

More recently, there has been an increasing interest in *closed-loop* active control methods that utilize real time information from the flow field to modify the behavior of actuation. This allows set-point tracking, as well as disturbance rejection, and crucially, it has the potential to stabilize a system about an unstable operating point, thus only requiring a small amount of energy input after transients as shown in several studies[2, 38, 13].

The feedback control approach chosen here is adjoint-based optimal control. This method consists in finding the control input that locally minimizes a cost function over a given time horizon. A key advantage of this method is that it does not require an a priori knowledge of the physical mechanism that will minimize the cost function, so it can be used to gain intuition about unsuspected but effective control strategies. For instance Joe *et al.* [19] applied optimal control to the flow over a separated flat plate with a jet located near the trailing edge and found that a phase locked, pulse-like waveform was optimal as it interacted with the vortices shed in the wake in a more efficient and robust way than sinusoidal forcing. Based on these results, Joe *et al.* [19] then designed a simple phase locked controller using a similar waveform, leading to a near-optimal performance, without the need for expensive estimators.

^{*}Corresponding author: t.flinois11@imperial.ac.uk

[†]Department of Aeronautics, Imperial College London, South Kensington Campus, London SW7 2AZ, UK

[‡]Department of Mechanical and Civil Engineering, California Institute of Technology, Pasadena, CA 91125, USA

Additionally, the cost of finding this optimal control does not increase regardless of the number of control inputs. For instance Bewley *et al.*[8] applied optimal control to re-laminarize a turbulent channel flow, where every point in the channel was used for blowing and suction. Finally, adjoint-based optimal control can be applied to steady and unsteady flows, as well as linear and nonlinear flows. Most other control approaches do not allow for such flexibility, especially with regards to the nonlinearity of the Navier-Stokes equations. In many contexts, this approach can therefore be seen as providing an upper limit on the achievable performance for a given control configuration. However, because in most cases the problem is nonlinear and non-convex, many studies have found that the results can be strongly influenced by the definition of the cost function[25, 8] and by the length of the optimization horizon[29, 23, 8]. The importance of carefully choosing the control problem definition is therefore investigated in this article.

In the present study rotation of the cylinder about its main axis is chosen as the control method. The experimental study of Tokumaru and Dimotakis[37] demonstrated the potential for this control method to affect the flow field and reduce the drag of a cylinder by up to roughly 80% at $Re = 1.5 \times 10^4$ and has prompted many other authors to study the effect of oscillatory cylinder rotation on the development of the vortex street at different Reynolds numbers, e.g. [11, 36, 32, 24, 6]. In these studies, the cylinder's sinusoidal rotation needs to be vigorous for the control to successfully reduce the drag: typically the amplitude of the tangential velocity on the cylinder surface is several times larger than the inflow velocity, and the frequency of the rotation is of the order of $St = fD/U_\infty = 1$, where f is the dimensional frequency. The open-loop rotation of the cylinder needs to be this powerful in order to change the wake's stability properties: the train of small vortices that are generated in each shear layer by the rotation and advected by the free-stream enhances the wake symmetry and suppresses the interaction between the shear layers. The associated form drag is therefore reduced significantly, but unsurprisingly, this actuation method uses more energy than it saves[7, 29].

He *et al.*[15] considered the optimal control of a cylinder wake at low Reynolds numbers using rotary oscillation. In their study, the optimal control was evaluated starting from the best open-loop sinusoidal configuration ($A=3$, $St=0.74$ for $Re = 200$, where A is the amplitude of the sinusoidally oscillating tangential surface velocity). They chose to find the periodic control waveform (with a several frequency components) that would minimize drag, based on a horizon of 3 (high-frequency) forcing periods, and a Reynolds number of 200 and 1000. The resulting waveform is qualitatively similar to the open-loop one (high amplitude and high frequency), but with marginally improved drag reduction. Homescu *et al.*[17] minimized the difference between the flow state and a target flow field, which was chosen to be the flow around the cylinder at $Re = 2$. They considered Reynolds numbers of 100 and 1000 for the constant and sinusoidal rotation case, and used horizons of up to 5 time units, which is roughly equivalent to one vortex shedding period. The optimal sinusoidal forcing parameters ($A=3.25$, $St=1.13$, for $Re = 100$) are different from the ones found by He *et al.*[15] but of the same order of magnitude. Protas *et al.*[28] considered a free waveform for the control and minimized the sum of the control power and the power required for overcoming drag, for Reynolds numbers of 75 and 150. They considered horizons of up to roughly one vortex shedding period. The resulting control waveform is discontinuous between each horizon so no clear physical mechanism was extracted to explain how the rotation affects the flow-field. Nevertheless, the drag is reduced by 7% and 15% for $Re = 75$ and 150 respectively, and with a positive energy balance. On the other hand, the amplitude of the control waveform does not seem to be changing significantly over time. Finally, Bergmann *et al.*[5, 4] used a reduced order model based on a Proper Orthogonal Decomposition of the flow-field. They chose to minimize the turbulent kinetic energy in the flow field and the mean drag of the cylinder at a Reynolds number of 200. As the cylinder rotation was constrained to be sinusoidal, the control converged towards the open-loop optimum.

In the present investigation the control waveform is not constrained in any way and the considered horizons are significantly longer than ones from previous studies (up to 100 time units). The effect of changing the cost function (minimizing squared lift or drag), the length of the optimization horizon (10 to 100 time units), and the Reynolds number (100 and 200) are considered. The numerical approach and problem setup is described in Sec. 2 and in Sec. 3 the optimal control results are analysed. The influence of the optimization parameters and in particular of the control horizon on the performance is also discussed in this section.

2 Problem formulation and numerical method

The two-dimensional incompressible Navier-Stokes simulations presented in this article were run using a finite-volume immersed-boundary fractional step algorithm developed by Taira and Colonius[35, 12]. For this study, linearized forward and adjoint solvers were developed based on the semi-discrete nonlinear

Table 1: Strouhal number of vortex shedding and mean drag coefficient of the unforced flow around a stationary circular cylinder with the nominal and refined set of parameters, compared with values obtained in previous studies.

Simulation	Re	Strouhal Number	Mean C_D
Nominal	100	0.163	1.330
Refined	100	0.164	1.327
Braza <i>et al.</i> [9]	100	0.16	1.36
Henderson[16]	100	0.166	1.350
Park <i>et al.</i> [26]	100	0.164	1.33
He <i>et al.</i> [15]	100	0.167	1.353
<hr/>			
Nominal	200	0.194	1.327
Refined	200	0.196	1.356
Braza <i>et al.</i> [9]	200	0.20	1.39
Henderson[16]	200	0.197	1.341
He <i>et al.</i> [15]	200	0.198	1.356
Bergmann <i>et al.</i> [5]	200	0.200	1.390

equations, expanding on earlier work of Joe *et al.*[19].

A nominal set of parameters was used in all simulations presented in this article. The adequacy of these parameters was therefore checked as summarized in Table 1. Here, the vortex-shedding Strouhal number and mean drag coefficient of a stationary two-dimensional circular cylinder in a free-stream with $Re = 100$ and $Re = 200$ were computed with the nominal parameters, as well as with a more refined set of parameters, and the results were compared to those found in the literature. For the nominal (refined) run the time step is 0.002 (0.001) and 8 nested grids are used, where each grid is composed of 240×120 (600×300) cells and the extent of the smallest grid is 4.8×2.4 (6.0×3.0) cylinder diameters. A good convergence and agreement with previous studies is obtained with the nominal set of parameters for both Reynolds numbers.

The adjoint-based optimization procedure considered in the present work aims to minimize a cost function of the form $J(x, \phi) = \int_0^T \mathcal{F}(x, \phi) dt$, which depends on the state (x) and control variables (ϕ). In this case, the integral of the squared lift or drag signals were used:

$$J_L = \int_0^T \frac{1}{2} L(t)^2 dt, \quad (1)$$

$$J_D = \int_0^T \frac{1}{2} D(t)^2 dt. \quad (2)$$

The cost function is minimized using a single degree of freedom but time-dependent control $\phi(t)$: The tangential velocity of the cylinder surface. Note that there is no control penalization term in (1) and (2) because a low amplitude, approximately zero-mean rotation is expected to (and turns out to be) optimal, usually resulting in a well-posed optimization problem.

In order to iteratively and locally minimize this cost function, the gradient of the cost with respect to the controls is determined in the standard manner[8, 19]: the cost is augmented to enforce the Navier-Stokes equations and the corresponding boundary conditions, using a set of Lagrange multipliers (the adjoint states). The augmented cost is then of the form $\tilde{J}(x, \phi, x^+) = \int_0^T \mathcal{H}(x, \phi, x^+) dt$, where x^+ is the adjoint state. Using calculus of variations, this procedure yields a set of conditions that must be satisfied in order to identify the optimal control: The Navier-Stokes equations (3) in vorticity form:

$$\begin{cases} \omega = \nabla \times (u \times \omega) - Re^{-1} \nabla \times (\nabla \times \omega) + \nabla \times f, \\ u_B = \phi(t) \hat{u}_t, \end{cases} \quad (3)$$

as well as the corresponding adjoint Navier-Stokes equations must hold throughout the simulation, while the gradient of the augmented cost function with respect to the controls $\partial \mathcal{H} / \partial \phi$ must be 0. Here u refers to velocity, $\omega = \nabla \times u$ to vorticity and $\dot{\omega} = \partial \omega / \partial t$, u_B is the velocity on the body surface, and $\phi(t)$ is the control, which, as mentioned above is tangential velocity on the body surface, mimicking cylinder rotation: \hat{u}_t is a unit vector at each immersed boundary point, pointing in the direction that is tangential to the body surface in the counterclockwise direction. The immersed body forces f are used

to impose the boundary condition on the body surface. Due to the similarity between the forward and adjoint equations, the adjoint solver is similar to the forward solver (except for the advection terms). Note however that the adjoint equations must run backwards in time starting from a “final condition”, (which is zero in the absence of a cost on the final state at $t = T$).

The control gradient is in general a non-zero vector of the dimension of the selected controls and is used to iteratively update the control waveform. In this case, it is therefore a vector with as many elements as there are time steps in the simulation and it can be shown that:

$$\frac{\partial \mathcal{H}}{\partial \phi} \propto f_t^+, \quad (4)$$

where f_t^+ is the component of the adjoint force at each immersed boundary point that is tangential to the body surface. The full adjoint optimization procedure can be outlined as follows:

1. A cost function, an initial control guess and a starting condition are defined;
2. The Navier-Stokes equations are solved starting from the initial condition and with the current control guess, and the corresponding cost is evaluated;
3. The adjoint equations are solved, and the control gradient $\partial H / \partial \phi$ is calculated from the results of the two simulations;
4. The optimal control update distance is calculated iteratively based on the calculated gradient, using a line minimization algorithm (more details below);
5. The control guess is updated according to the results of the line minimization and the new cost is evaluated;
6. Steps 2. to 5. are repeated until convergence, using updated controls each time;
7. The starting time is advanced by 2/3 of the control horizon (in this case) and the state of the controlled flow field at that time is used as the new initial condition. The last third of the converged optimal control signal is discarded. The new initial control guess is also chosen (set to zero in this case);
8. Steps 1. to 7. are then repeated for the next horizon.

More details about this procedure are included for instance in[8, 19, 28].

The line minimization algorithm mentioned in the 4th step above is necessary as the control gradient only provides information about the direction in which the control needs to be updated in order to optimally reduce the cost function (locally). A further inner iteration is then required to find the optimal *magnitude* of the control update in the gradient direction. A steepest gradient algorithm can be used, but it is more efficient to use a conjugate gradient approach[27]. Typically, a Brent line minimization is then used to find the optimal update distance[27]. However, in order to make this searching procedure more efficient, a parallel version of the Brent’s search algorithm was developed and this procedure is described in more details in Appendix A;

The *fully continuous* adjoint equations corresponding to (3) are:

$$\begin{cases} -\dot{\omega}^+ = \nabla \times (\omega_0 \times u^+) - \nabla^2 (u^+ \times u_0) - Re^{-1} \nabla \times (\nabla \times \omega^+) + \nabla \times f^+, \\ u_B^+ = u_{slip}^+, \end{cases} \quad (5)$$

where $^+$ refers to adjoint quantities, $_0$ to base flow quantities and u_{slip}^+ is the adjoint slip velocity at the body surface. In this case it can be shown that $u_{slip}^+ \propto f_y$ for (1) and $u_{slip}^+ \propto f_x$ for (2), where f_x and f_y are respectively the x and y components of the local force (from the forward simulation) on each immersed boundary point on the body. Solving a discretization of (5) would only lead to the discrete adjoint solution in the limit of infinite temporal and spatial resolution. Instead, the spatially-discrete but temporally-continuous adjoint equations were implemented. As the base flow is unsteady, the time-stepping scheme is not self-adjoint. Additionally, the same nested grid procedure was used in the forward and adjoint solver, but this procedure is in fact not self-adjoint either, as noted by Ahuja and Rowley[2]. Finally, solving the adjoint equations requires storing the entire solution of the forward problem (the unsteady base flow). To reduce the computational requirements of this procedure, we only store every 10th snapshot of the forward solution and use linear interpolation to reconstruct it at a cheaper cost. As

Table 2: Summary of results from the optimizations: the horizon length is given in convective time units, J refers to the cost functions defined in Eq. (1) for ‘‘Lift’’ and Eq. (2) for ‘‘Drag’’, Re is the Reynolds number, and C_D is the drag coefficient. The quoted drag reduction percentage is calculated with respect to the mean unforced drag at the corresponding Reynolds number and is estimated from the mean value at which the drag settles towards the end of the horizon. Note that several horizons were used in Runs 2, 6 and 9 and all horizons where started with a zero initial control guess.

Run	Horizon Length	J	Re	C_D	Reduction
1	50	Drag	100	17%	
2	2×50	Drag	100	19%	
3	100	Drag	100	14%	
4	50	Lift	100	6%	
5	50	Drag	200	10%	
6	2×50	Drag	200	10%	
7	100	Drag	200	7%	
8	50	Lift	200	10%	
9	10	Drag	100	> 60%	

a consequence, the gradients computed with this code are not the exact discrete gradients of the forward problem, so we can only expect to obtain an approximation to the exact discrete optimal solution of the problem.

In order to check that the gradients obtained with the code are of an acceptable accuracy, a standard finite-difference check[17] was performed on the adjoint code: if the forward and adjoint equations are satisfied, then the following Taylor expansion of the cost function can be written:

$$\tilde{J}(\phi) - \tilde{J}(\phi + \delta\phi) = \int_0^T \left(\frac{\partial \mathcal{H}}{\partial \phi} \delta\phi + O(\delta\phi^2) \right) dt, \quad (6)$$

where the nominal control is chosen to be $\phi(t) = 0$ and $\delta\phi$ is an arbitrary control perturbation, chosen to be a sinusoidal function of the form $\delta\phi = \epsilon \sin((2\pi St)t)$, for small enough ϵ and here Strouhal numbers in the range $0.1 \leq St \leq 0.5$ were tested. The relative error at $Re = 100$ between the two sides of Eq. (6) – i.e. (normalized by $\tilde{J}(\phi) - \tilde{J}(\phi + \delta\phi)$) – is typically of the order of 0.5%, 1% and 3% for $T = 10$, $T = 50$, and $T = 100$, respectively. Due to the fact that the error increases with T , we can expect to obtain slightly more suboptimal results with longer horizons.

3 Results and discussion

Several optimizations were run in order to investigate the influence of changing the cost function, the horizon length and the Reynolds number, as summarized in Table 2. The performance of the optimizations is quantified by estimating the amount of sustained drag reduction obtained towards the end of the converged simulations.

3.1 Suppression of vortex shedding

In this section we first provide an analysis of the best optimal control results (Run 2), before discussing the influence of the different parameters on the overall optimization performance. Figure 1(a) is the unforced flow-field and is compared to the optimally controlled flow field in Fig. 1(b). The intensity of the vortex shedding in Fig. 1(b) is reduced and the flow appears to be much more symmetric. The optimal control signal is shown in Fig. 2(a), while the optimally controlled drag and lift coefficient signals are shown in Fig. 2(b) and (c) respectively. In Fig. 2(a), the drag of the unstable (steady) equilibrium is also plotted (this value was computed by using Selective Frequency Damping[20, 1]). Clearly, the controlled flow-field has been stabilised to a drag state that is close to that of this equilibrium.

From Fig. 1, Fig. 2 and Table 2, it is clear that in Run 2 the vortex shedding is almost fully suppressed and that the lift oscillations and the mean drag are both reduced significantly. Moreover, towards the end of the second optimization window, the tangential velocity on the cylinder surface is of the order of 0.1% of the incoming flow velocity. Comparing these results to previous work with similar setups, only Protas

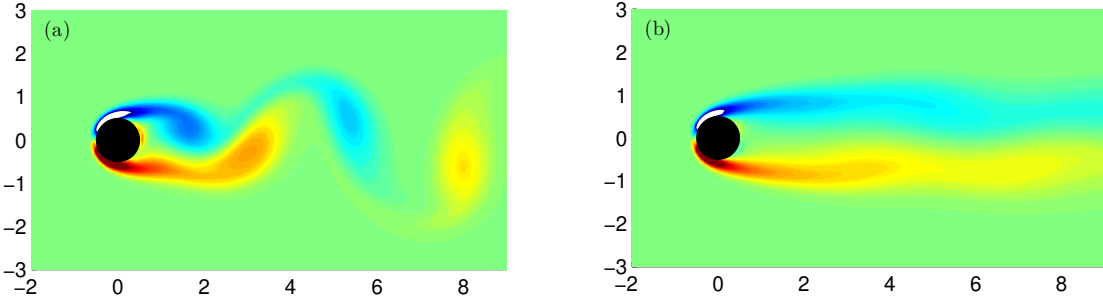


Figure 1: (Color Online) Results from Run 2. (a) Unforced wake vorticity contours. (b) Optimally controlled wake vorticity contours. The intensity of the vortex shedding is clearly reduced in the controlled case.

et al.[28] obtained comparable drag reductions without needing an excessively large amount cylinder rotation. However, the control waveform obtained by Protas *et al.*[28] is discontinuous due to the chosen setup for the optimizations: only short optimization horizons were used. In the present case, almost no cylinder rotation is required to keep the Von Kármán wake suppressed for large times. Moreover, we obtain a smooth control waveform, which clearly has a main frequency component that corresponds to the vortex shedding frequency. We therefore proceed to investigate in what way the wake is affected by the control.

In previous optimal control studies[15, 17, 4], the aggressive optimal control obtained can be seen as essentially an open-loop strategy with optimized (constant) parameters: purely harmonic forcing cannot suppress the wake instability, it can only alter it to a more favorable drag state with suitably large rotational velocities. In order to test whether the low drag state reached with optimal control can also be obtained with similar open-loop control signals, two open-loop control waveforms that approximate the optimal control were designed, as shown in Fig. 3: the first is a sinusoidal signal whose frequency, amplitude and phase approximately match the optimal control at $t = 0$ and the second is an exponentially decaying sinusoidal waveform (also with approximately matching frequency, amplitude and phase at $t = 0$). Upon applying these control signals to the cylinder, the drag is initially reduced in both cases, but it returns to its unforced value for the exponentially decaying sinusoidal case. In the sinusoidal case the control actually increases the drag by 9% for large times, with respect to the unforced case. This type of behavior is common in flows where the vortex shedding frequency naturally locks-on to the forcing frequency when it is close to the unforced shedding frequency, and is thereby amplified by it (e.g. [14]).

These simple tests therefore seem to confirm that there is an intrinsic need for feedback information to be available to the control for it to damp the vortex shedding effectively. Thiria[36] studied the influence of the rotation of the cylinder on the wake vorticity in the *open-loop* case and argued that when the optimal drag reduction forcing parameters are chosen, the rotation of the cylinder has a “destructive” influence on the formation of vortices, since the cylinder rotation creates vorticity of the *opposite* sign to that of the vortex being formed. At the same time, the rotation promotes the creation of a vortex in the opposite shear layer, thus effectively enhancing the synchronization of the shedding of vortices in the wake. On the other hand, when the rotation is locked-in with the vortex shedding, the interaction can be seen as “constructive” since the cylinder rotation creates vorticity of the *same* sign as that of the vortex being formed and reduces the amount of vorticity in the opposite shear layer, thus aggravating the shear layer interaction and strength of the vortices.

Comparing the direction of the rotation with the vortex shedding phase for the open-loop sinusoidal case described above (black dashed line) it is clear that the same conclusions can be drawn: as shown in Fig. 4(a) and (c), for $t < 10$, the rotation is always in the “destructive” direction, while for late times $t > 60$, (Fig. 4(b) and (d)) the vortex shedding is locked-in and the rotation is in the “constructive” direction. This suggests that matching the cylinder’s rotation direction to the phase of the vortex shedding is a promising strategy to suppress the wake fluctuations without requiring the full optimal control framework.

One way to interpret this conclusion is that the mechanism leading to the suppression of vortex shedding in the open-loop experiments of Tokumaru and Dimotakis[37] and the subsequent related studies is effectively the same as the one allowing suppression of vortex shedding in the energy-efficient closed-loop case. The main difference between the open-loop and closed-loop cases is that a large amount of input energy is required with sinusoidal forcing in order for the destructive rotation-vortex shedding interaction

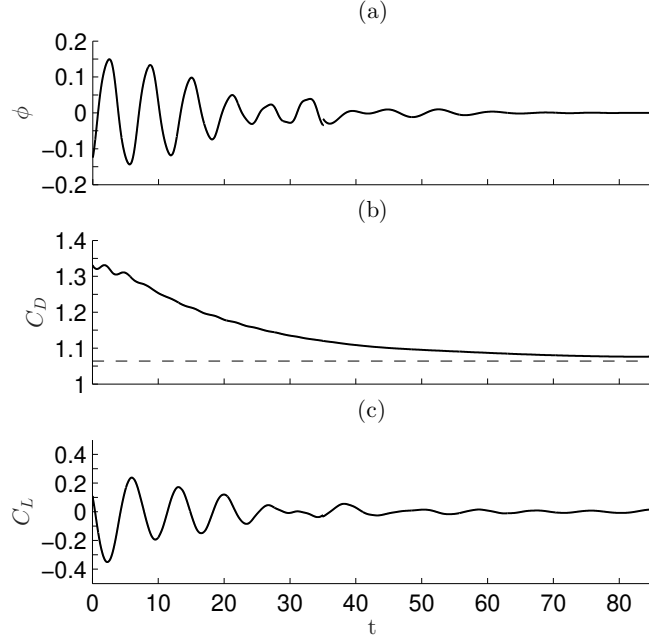


Figure 2: Results from Run 2: (a) Optimal control waveform and resulting drag (b) and lift (c) coefficients, showing a clear suppression of the lift oscillations, a significant reduction in the mean drag and a control waveform that tends to nearly zero amplitude for large times. In (b) the drag of the unstable equilibrium of the flow-field, computed by using Selective Frequency Damping[20, 1], is also plotted as a reference (dashed line).

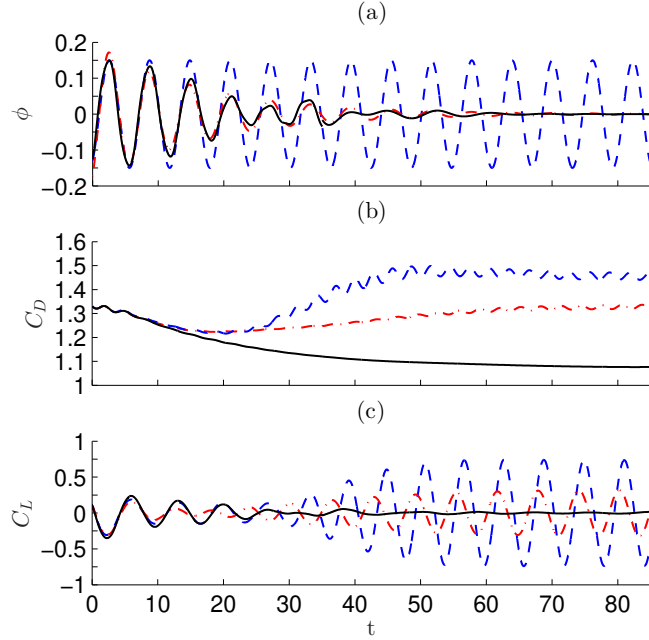


Figure 3: (Color Online) Results using harmonic approximations to the optimal control waveform of Run 2 (also run with $Re = 100$): (a) Control signals and resulting (b) drag and (c) lift coefficients. Black solid line: optimal control. Red dash-dotted line: exponentially damped sinusoidal forcing. Blue dashed line: sinusoidal forcing. Despite a similar initial behavior, neither of the open-loop approximations are able to suppress the shedding sustainably.

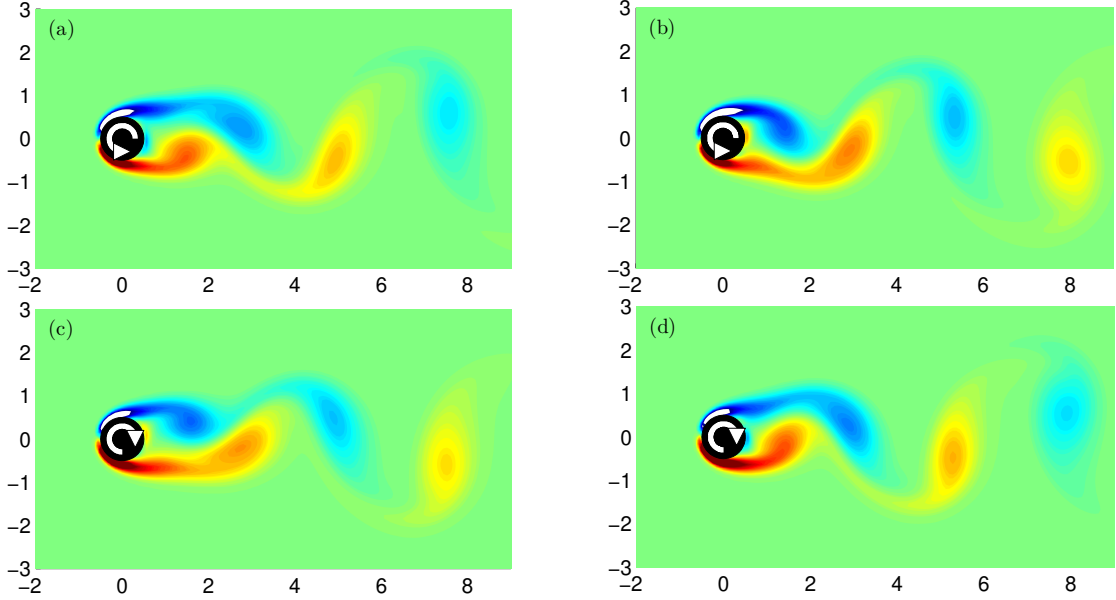


Figure 4: (Color Online) Vorticity contours for the sinusoidal forcing case with amplitude, frequency and phase matching the optimal control for early times. (a,b) Maximal value of positive (anti-clockwise) rotation. (c,d) Maximal value of negative (clockwise) rotation. (a,c) In the first few shedding periods, the cylinder rotation is “destructive” and reduces the intensity of the shedding. (b,d) Once lock-in occurs, the rotation becomes “constructive” and reinforces the shedding.

to become stable. On the other hand, similar performance is possible with a much smaller control effort if information is fed back to the controller as this allows the unstable destructive interaction to be maintained without requiring the fast high amplitude rotation that is necessary with open-loop forcing.

3.2 Impact of optimization and simulation parameters

The results in Table 2 show that at a Reynolds number of 100, minimizing the RMS drag is more efficient in this case than minimizing the RMS lift (see Runs 1 compared to Run 4). For a Reynolds number of 200 however, the performance is comparable. For both cost functions and Reynolds numbers, the cylinder rotation is slow, of small amplitude and roughly at the vortex shedding frequency and the drag is significantly reduced due to the suppressed intensity of vortices in the wake. In previous adjoint optimization studies (e.g. [25, 8]) it was also found that it is not always immediately obvious why one cost function performs better than another one, due to the non-convexity and nonlinearity of the problem. Clearly here, we expect both cost functions to be minimized if the vortex shedding is somehow completely suppressed, but there is no guarantee that using the two cost functions will in fact lead to similar modifications in the flow field, as the local minimum reached may be different. The present results therefore bring a further confirmation that it is worth running an optimization with several cost functions even if all of them are expected to be reduced simultaneously by the desired flow-behavior.

As may be expected, increasing the Reynolds number is consistently detrimental to the relative performance of the control as shown in Table 2. From linear stability analysis[18], the real part of the unstable eigenvalues associated with the vortex shedding grows with the Reynolds number and several studies[22, 24] also reported a reduction of closed-loop performance as the Reynolds number increased. In the present case, the two shear layers are more unstable for $Re = 200$ than $Re = 100$, so even if the cylinder rotation is able to initially enhance the symmetry of the wake and delay the interaction between the shear layers, the instability is not as readily suppressed for the entire wake region and the drag reduction is therefore not as significant.

A key difference between previous work and the setup chosen here is that in this study, it was chosen to use much longer optimization horizons. Protas *et al.*[28] found that the horizon length should be longer than one vortex shedding period but that only marginal improvements can be obtained by further increasing it. Furthermore, Bewley *et al.*[8] argued that if the horizon is too long horizons the optimization can become excessively non-convex and computationally expensive, leading to suboptimal performance in practice. Furthermore, inaccuracies in the computed gradient have the potential to stall

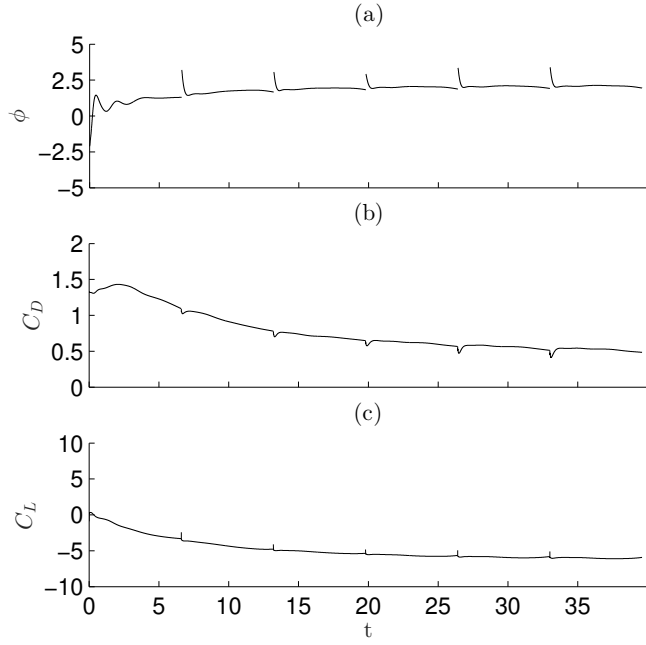


Figure 5: (a) Optimal control waveform for several receding horizons of 10 convective time units and resulting (b) drag and (c) lift coefficients respectively. The last 1/3 of each horizon is discarded. The cost function is given by Eq. (2) and $Re = 100$. The optimal control leads to a non-zero-mean, fast rotation optimum.

the optimization for very long horizons, leading to worse approximations to the exact discrete optimum. In this article, optimizations with horizon lengths of 10, 50 and 100 time-units were run.

Considering first the 100 time-unit optimizations, a similar behavior to the 50 time unit case can be seen in Table 2, but with an inferior performance (see Run 2 and 6 compared to 3 and 7). This correlates well with the fact that 100 time units is indeed an excessively long horizon in this case. The simulations were run for 20 optimization iterations in all cases here, and further iterations may result in a further cost reduction, but the present results confirm that such long horizons can indeed result in prohibitively slow convergence of the optimization problem.

In order to obtain optimization results that are longer than one horizon when the horizon length is smaller than 100 time units, a new initial control guess and starting condition are necessary to start the optimization at each horizon. As mentioned in Sec. 2, the initial condition for each horizon i of total length T_i was chosen to be a snapshot of the converged solution of the previous horizon $i - 1$ such that $t_i(0) = (2/3)T_{i-1}$. For the initial control guess, it was chosen to set the control to zero rotation throughout the horizon, thus leading to an initial discontinuity since $\phi((2/3)T_{i-1}) \neq 0$ in general.

When the horizon length is 1 time unit (not shown here), i.e. shorter than a vortex shedding period, it was found that the problem does not converge at all, as it is ill-posed from the first optimization horizon, without a control penalty term. With a horizon length of to 10 time units however, the solution of the optimization tends towards a well-known low-drag flow-state with *constant* rotation, as shown in Fig. 5. The control waveform has discontinuities at the start of each horizon but the general behaviour of the control is still clearly visible. Homescu *et al.*[17] and Kang *et al.*[21] also showed that the cylinder drag can be reduced significantly and the vortex shedding suppressed completely by using sufficiently fast constant rotation of the cylinder in one direction. Unsurprisingly, this results in a significant constant lift force on one side of the cylinder, as shown in Fig. 5(c). Both studies found an optimal rotation rate at $Re = 100$ of $\phi \approx 1.85$. Here the rotation rate quickly increases until it reaches a value that is close to this optimum, but then continues to slowly increase. After 40 time units, the rotation rate is $\phi \approx 2.1$ and the cylinder is still slowly accelerating. It is expected that computing further horizons would lead to a continued increase in this quasi-steady rotation rate, since the drag decreases further for even higher rotation rates[21]. It is therefore clear from these results that once again, the physical mechanism reducing drag and stabilizing the wake is effectively an open-loop strategy, which does not require closed-loop control but does require a significant amount of input energy.

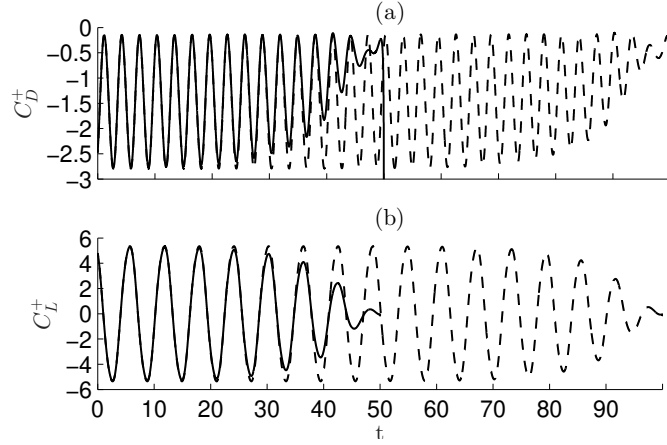


Figure 6: Time history of the adjoint force coefficients for the first optimization iteration (no cylinder rotation in the corresponding forward run) of Run 1 (solid line) and Run 3 (dashed line). (a) Adjoint drag C_D^+ , (b) Adjoint lift C_L^+ . Approximately 25 convective time units are required for the two curves to overlap, which is significantly larger than a vortex shedding period.

These results show that the choice of horizon length can have a crucial impact on the solution of the optimization and suggest the existence of another important timescale than the vortex shedding frequency. It seems reasonable to expect a control that efficiently suppresses vortex shedding to do so over a length of time that is longer than one vortex shedding period. For instance a control waveform that eventually fully stabilizes the wake will not necessarily lead to the maximum drag reduction in the first few time units.

One way to visualize this time scale is to realize that the adjoint flow field – even if based on a fully periodic limit-cycling base flow – will be a transient simulation. From a numerical point of view, given that the gradient of the controls is always based both on the forward and adjoint state, the horizon should be long enough for the gradient at the start of the simulation not to be significantly affected by any further increase in the horizon length. Comparing the forces of the adjoint simulation from the first iteration of Run 1 to those of Run 3 (Fig. 6) shows that the adjoint simulation experiences “transients” for roughly the first 25 time units before the two sets of forces overlap (recall that the adjoint simulation runs backwards in time).

For the last 25 time units of the horizon, the control will be therefore optimized according to what can be considered to be a “short term” control strategy, which may not be sustainable. In some cases, having several short horizons might just lead to a suboptimal but similar control waveform to the long horizon case, but in others, the two physical mechanisms leading to a reduction in the cost might be different altogether (as with the 10 time-unit horizons here). Note however, that in this case there is no guarantee of which technique will have the lowest cost since the control simply tends towards two different local minima (indeed, the drag is reduced more with the fast constant rotation than with the oscillatory rotation in this case).

4 Conclusions

In this article, optimal control is applied to the flow over a cylinder, where the mean-squared lift or drag were minimized using unconstrained rotation of the cylinder. The optimization horizons were chosen to be longer than in previous studies, where they typically are at most of the order of a vortex shedding period. In order to speed up the optimizations, a parallel equivalent of the Brent line-minimization algorithm was introduced, which significantly reduces the time required for the line minimization part of each optimization iteration if several forward simulations can be run in parallel.

It was shown that at Reynolds numbers 100 and 200, cylinder rotation can effectively suppress vortex shedding in the wake. The optimal control waveform was found to be phase-locked with vortex shedding, and the rotation is always applied in a direction that weakens the vortices shed in the wake. The stabilizing action of the control on the wake is therefore similar to the high-amplitude and high-frequency open-loop optimum that is well documented in the literature, but feedback vastly reduces the required

rotation rate.

It was found that this phase locking behavior can only be achieved in a closed-loop control setting. Applying an almost identical but harmonic (i.e. open-loop) forcing signal instead results in a drift between the forcing and shedding phase, and eventually in an increased drag. On the other hand the optimal forcing decreases the drag by up to 19% compared to the unforced case and the amplitude of the actuation required to keep the flow in this stabilized state approaches zero, with tangential velocities on the cylinder surface of the order of 0.1% of the inflow velocity towards the end of the considered optimization window. This shows the importance of keeping the control waveform fully unconstrained, as previous studies where only periodic solutions were allowed obtained the high-amplitude and frequency open-loop optimum rather than the stabilizing control obtained here.

The analysis of the different optimization parameters confirmed the fact that the setup of the optimization – including the choice of cost function and horizon length – can strongly affect the final results. In particular, changing the horizon length can even change the local minimum that is identified and hence the mechanism through which the cost function is minimized. In this case, it was found an optimization window longer than the vortex shedding frequency was required in order for the converged optimal control to stabilize the wake in an efficient manner. It was found that the transients of the adjoint simulation can provide some important information regarding the adequacy of the chosen horizon length. If the horizon is long enough, the state of the adjoint solution and hence the control gradients will not be strongly affected by any further increase of the horizon length. On the other hand, if the horizon is too short, this can result in a “short term” optimization, whereby the reduction in the cost must be measured quickly but may be different from the “long term” optimum. In this case, with horizons of 10 time-units, the drag was minimized with a fast, nearly constant rotation of the cylinder, whereas with longer horizons of 50 time-units or more, the low amplitude, approximately zero-mean, oscillatory rotation of the cylinder described above was obtained.

A Parallel line minimization

Brent’s method[27] can be used to minimize a cost function by varying one parameter only, say α , and where each evaluation of the cost is expensive and no gradient information is available. Clearly this is the case here, where the parameter is the amplitude of the control update in the optimal gradient direction, so each evaluation of the cost corresponds to a full forward simulation. However, in situations where several forward simulations can be run in parallel, evaluating the cost for several parameter values can take the same time as evaluating one. Note that only the resulting costs need to be communicated between the jobs at the end of the simulations. We therefore seek to develop a parallel equivalent to Brent’s method, which takes advantage of the possibility to run p jobs simultaneously.

There are two main steps in the serial algorithm. First, one attempts to find three values of the independent parameter $\alpha_1 < \alpha_2 < \alpha_3$ that bracket a minimum, i.e. $J(\alpha_2) < J(\alpha_1)$ and $J(\alpha_2) < J(\alpha_3)$. This is usually done by evaluating costs corresponding to parameter values that are exponentially large (following an unstable geometric progression) until a minimum is found. Here instead of evaluating each cost sequentially, we can accelerate this procedure up to p times by simply evaluating the next p terms in the geometric sequence in parallel.

In the second step of the original method, the size of this bracket is reduced iteratively until convergence during the minimization procedure, using one of two methods. In the first method, we evaluate the parameter value corresponding to the minimum of the parabola that fits through the three bracket points (this method can converge quickly but is not always robust). The second method is the golden section search, whereby the next α value is chosen such that the two possible brackets that can be obtained for the next iteration are of equal size (this method is slower but always converges).

In the original algorithm, an intricate set of rules for choosing which method to use for every iteration is defined. Here, we can use a similar set of rules, but instead we will only decide whether or not to use 1 of our p jobs to evaluate the parabola’s minimum. A parallelized version of the golden line search is then always applied to the remaining $n = p - 1$ or $n = p$ jobs. In total, we therefore always evaluate simultaneously p different values of α at each iteration, instead of just one. We then keep the 3 values of α that correspond to the smallest bracket of the minimum for the next iteration of the algorithm.

The simplest way of choosing the n values of α to evaluate within the bracket is to ignore the fact that we already know a minimum in the bracket and just split the bracket equally. This will result in brackets of equal size for the next iteration as required: each bracket will be $2l/(n + 1)$ long, where l is the initial bracket length. For large n , discarding the knowledge of the current minimum value will only have a small impact, but for $n = 1$ the bracket is not reduced at all since $2l/(n + 1) = l$. For $n = 2$ we

have $2l/(n+1) \approx 0.667l$, whereas the optimal serial golden section search results in a smaller bracket with only one cost evaluation: $(\sqrt{5}-1)l/2 \approx 0.618l$ (see Fig. 7).

A more efficient approach is to use a similar rationale to the golden section search, by choosing to evaluate the cost corresponding to α values that make all resulting brackets of equal size regardless of where the minimum lies, but also taking into account the fact that one value inside the bracket (the current minimum guess) is already known from the previous iteration. In order for all the possible brackets to be of equal size, the distance between α values must alternate between two values L_1 and L_2 , such the resulting bracket for the next iteration is always $L_1 + L_2 = L_2 + L_1$ long. We therefore only need to identify L_1 and L_2 regardless of the value of n : given a bracket defined by the three α values: $[\alpha_0, \alpha_0 + x, \alpha_0 + l]$, where the current minimum guess is at $(\alpha_0 + x)$, and the bracket is l long, we define the $(n+3)$ parameter values $(\alpha_0 + l_i)$ for $0 \leq i \leq n+2$ such that:

$$l_{i+1} = \begin{cases} l_i + L_1 & \text{for even values of } i, \\ l_i + L_2 & \text{for odd values of } i, \end{cases}$$

for some $L_1 > 0$ and $L_2 > 0$ and where $l_0 = 0$. It follows that n values of α need to be evaluated since we have $[l_0, l_1, l_{n+2}] = [0, x, l]$ for some value of $0 < i < n+2$ so the three corresponding costs are already known from the current bracket values.

If n is even, then the values of L_1 and L_2 are:

$$\begin{aligned} L_1 &= \text{mod}(x, L), \\ L_2 &= L - L_1, \end{aligned}$$

where $L = 2l/(2+n)$, $\text{mod}(x, L) = x - L \text{ floor}(x/L)$ and $\text{floor}(x/L)$ refers to the closest integer smaller or equal to x/L . In the special case where x is exactly a multiple of L (i.e. $\text{mod}(x, L) = 0$ or L), in order to avoid having $L_1 = 0$ or $L_2 = 0$, we instead define: $L_1 = L_2 = l/(2+n)$, which is also a solution in this case.

Proof. If n is even, then the full interval l is split into $(n+2)/2$ intervals of size L_1 and $(n+2)/2$ intervals of size L_2 :

$$\frac{n+2}{2}L_1 + \frac{n+2}{2}L_2 = l,$$

and therefore $L_1 + L_2 = 2l/(n+2) = L$, which does not depend on x . Additionally, we need x to be exactly at the end of one of these intervals, and since we start with an L_1 interval by definition, x can most likely be written:

$$k(L_1 + L_2) + L_1 = x,$$

for some value of $0 \leq k < (n+2)/2$ to be determined. If we now write $x = mL + y$, where $m = \text{floor}(x/L)$ and $y = \text{mod}(x, L)$, then $mL < x < (m+1)L = mL + L_1 + L_2$. Since the next interval after mL is always an L_1 interval, we must have: $L_1 = y$, and therefore $m = k$, and $L_2 = L - L_1$. In the unlikely case where $y = 0$ exactly, we obtain:

$$(k+1)(L_1 + L_2) = x = mL,$$

and therefore we are free to choose where we cut L to form L_1 and L_2 . By choosing $L_1 = L_2 = L/2$ the interval is sampled as uniformly as possible. \square

If on the other hand n is odd, then a slightly more complicated procedure is required:

$$\begin{aligned} L_1 &= \begin{cases} (n+1)y/(n+1-2m) & \text{if } x < (m+1)l^*, \\ (n+1)(L-y)/(2m+2) & \text{if } x > (m+1)l^*, \end{cases} \\ L_2 &= L - \frac{n+3}{n+1}L_1, \end{aligned}$$

where we define:

$$\begin{aligned} L &= \frac{2l}{n+1}, \\ l^* &= \frac{2l}{n+3}, \\ m &= \text{floor}(\frac{x}{L}), \\ y &= \text{mod}(x, L), \end{aligned}$$

so that $x = mL + y$. The unlikely cases where x is an exact multiple of L (i.e. $\text{mod}(x, L) = 0$) or of l^* (i.e. $\text{mod}(x, l^*) = 0$) result in $L_1 = 0$ and $L_2 = 0$ respectively. For such values of x , there is no set of parameter values l_i that satisfies the conditions of having equal sized brackets, while ensuring that $[l_0, l_i, l_{n+2}] = [0, x, l]$ for some value of $0 < i < n + 2$. Therefore, one can simply discard x and just revert to splitting the bracket into intervals of equal size such that $L_1 = L_2 = l/(1 + n)$.

Proof. Since the first interval is L_1 by definition, the interval must be split so that:

$$\frac{n+3}{2}L_1 + \frac{n+1}{2}L_2 = l, \quad (7)$$

and thus

$$L_2 = L - \frac{n+3}{n+1}L_1. \quad (8)$$

Additionally, we need x to be exactly at the end of one of the intervals, so depending on the location of x , we will have either:

$$k(L_1 + L_2) + L_1 = x,$$

for some value of $0 \leq k < (n+1)/2$ to be determined, or

$$(k+1)(L_1 + L_2) = x.$$

In the first case, using Eq. (8), this will lead to $L_1 = (n+1)(x - kL)/(n+1 - 2k)$, and in the second to $L_1 = (n+1)(L + kL - x)/(2k + 2)$.

Equation (7) can be reformulated as: $L_1 + L_2 = L - 2/(n+1)L_1$ and this linear relationship means that $0 < L_1 < l^*$ and $0 < L_2 < L$. Furthermore:

$$\begin{aligned} \min_{x \in [0, l]} L_1 + L_2 &= L - 2/(n+1) \max_{x \in [0, l]} L_1 = l^*, \\ \max_{x \in [0, l]} L_1 + L_2 &= L - 2/(n+1) \min_{x \in [0, l]} L_1 = L, \end{aligned}$$

and as a result we have:

$$l^* < L_1 + L_2 < L. \quad (9)$$

Again using Eq. (7), for any integer i such that $0 \leq i < (n+1)/2$, we can write:

$$i(L_1 + L_2) + L_1 = iL + \left(1 - \frac{2i}{n+1}\right) L_1,$$

and as a result:

$$\begin{aligned} iL &< i(L_1 + L_2) + L_1 \\ &< iL + \left(1 - \frac{2i}{n+1}\right) l^* = (i+1)l^*. \end{aligned} \quad (10)$$

Finally combining Eq. (9), Eq. (10):

$$\begin{aligned} iL &< i(L_1 + L_2) + L_1 \\ &< (i+1)l^* \\ &< (i+1)(L_1 + L_2) \\ &< (i+1)L. \end{aligned} \quad (11)$$

If we again adopt the notation: $x = mL + y$, then unless $y = 0$, we can always write $mL < x < (m+1)L$. If $x < (m+1)l^*$, then $mL < x < (m+1)l^*$, so using Eq. (11) we have: $m(L_1 + L_2) < x < (m+1)(L_1 + L_2)$. Therefore, x must be of the form $x = m(L_1 + L_2) + L_1$, so this is the first case mentioned above with $k = m$ and hence:

$$L_1 = (n+1)y/(n+1 - 2m).$$

If on the other hand, $x > (m+1)l^*$, then we get $(m+1)l^* < x < (m+1)L$, which leads to $m(L_1 + L_2) + L_1 < x < (m+1)(L_1 + L_2) + L_1$ and hence x must be of the form: $x = (m+1)(L_1 + L_2)$. This corresponds to the second case again with $k = m$ and:

$$L_1 = (n+1)(L-y)/(2m+2).$$

From Eq. (7), $L_1 = 0$ occurs when $L_2 = L$, which corresponds to $\text{mod}(x, l^*) = 0$ and conversely, $L_2 = 0$ occurs when $L_1 = l^*$, which corresponds to $\text{mod}(x, L) = 0$. In both of these cases, there is no way to split l equally into intervals of size L_1 and L_2 and have one of the intervals end exactly at x , the current minimum value. We can therefore revert to splitting the interval equally in this case. \square

For even values of n , the length of the next bracket always becomes $L_1 + L_2 = L = 2l/(n+2)$ and this is therefore more efficient than discarding the current minimum and splitting the interval equally (especially for small n), as mentioned above and shown in Fig. 7 since $2l/(n+2) < 2l/(n+1)$. For odd values of n , using Eq. (9): $2l/(n+3) < L_1 + L_2 < 2l/(n+1)$. In practice, the performance varies throughout this range.

Figure 7 outlines the performance of the method by showing the size of the bracket of the next iteration for different number of jobs run in parallel n , and by comparing the performance of this method to both the optimal serial golden section search and the “equal split” method (where the current minimum value is discarded). The efficiency of the parallel method is clear: running $n = 4$ jobs simultaneously leads to a bracket that is smaller than the serial golden line search bracket obtained after two iterations, and similarly running $n = 6$ jobs simultaneously is almost three times as efficient as running just one, for the same total running time.

Note that with the serial Brent line search, it is clearly not acceptable to obtain a bracket of size $2l/(n+1) = l$. The algorithm is therefore constructed so that the aspect ratio of the bracket is constant and equal to $\min(x, 1-x) = (3 - \sqrt{5})l/2$ (i.e. the so-called “golden ratio”) as often as possible. The next bracket size is then $(\sqrt{5} - 1)l/2 \approx 0.618l$, which is closer to $2l/(n+3) = l/2$ than $2l/(n+1) = 1$. When the previous bracket was obtained with a parabolic fit, the algorithm attempts to recover the golden ratio and this results in both possible brackets not being of the same size: in the worst case the largest bracket is of size $(5 - \sqrt{5})l/4 \approx 0.691l < l$, which is just larger than $2l/(2+n) = l/3$, so still satisfactory.

In the parallel case, stationary points that ensure the conservation of the bracket aspect ratio between iterations also exist, both for even and odd n . For even n , these points are at:

$$\begin{aligned} x_1(k) &= kl/(1-L) & \text{where } 0 < k < n/2, \\ x_2(k) &= L(1+k)/(1+L) & \text{where } 0 \leq k < (n+2)/2, \end{aligned}$$

and as before $L = 2l/(n+2)$. However, as the largest next bracket is of size L regardless of the location of x , having a constant bracket aspect ratio does not speed up the convergence for even n .

For odd n on the other hand, this may be more useful. The values of x that ensure a constant bracket aspect ratio are the roots of the following polynomials:

$$\begin{aligned} 2x_1^2 + x_1(n-1) - 2k &= 0, \\ 2x_2^2 - x_2(n+5) + 2(k+1) &= 0, \end{aligned}$$

as well as $(l - x_1(k))$ and $(l - x_2(k))$. These roots are:

$$\begin{aligned} x_{1\pm}(k) &= \frac{n+5 \pm \sqrt{-16m + n^2 + 10n + 9}}{4}, \\ x_{2\pm}(k) &= \frac{1-n \pm \sqrt{16m + (n-1)^2}}{4}. \end{aligned}$$

Only the roots that yield $0 < x < l$ are relevant and these correspond to $x_{1+}(k)$ and $(l - x_{1+}(k))$ for $0 < k < (n+1)/2$ and $x_{2-}(k)$ and $(l - x_{2-}(k))$ for $0 \leq k < (n+1)/2$. The value of x that always yields the smallest bracket corresponds to $x_{2-}(0)$, leading to a bracket of size $(\sqrt{n^2 + 10n + 9} - n - 1)/(2n + 2)$. This “optimal” performance for odd n is plotted in Fig. 7, which shows that the next bracket size is always between $2l/(n+2)$ and $2l/(n+3)$ (better than the even n convergence). Additionally, the larger the value of n , the closer the optimal value gets to $2l/(n+3)$. If a purely parallel golden section search algorithm is used this would represent a significant improvement over the worst case of $2l/(n+1)$. However, when using the full parallelized Brent line search, the number of jobs run using the parallel golden line search changes between $n = p$ and $n = p - 1$ depending on whether one job is used for the parabolic fit so it

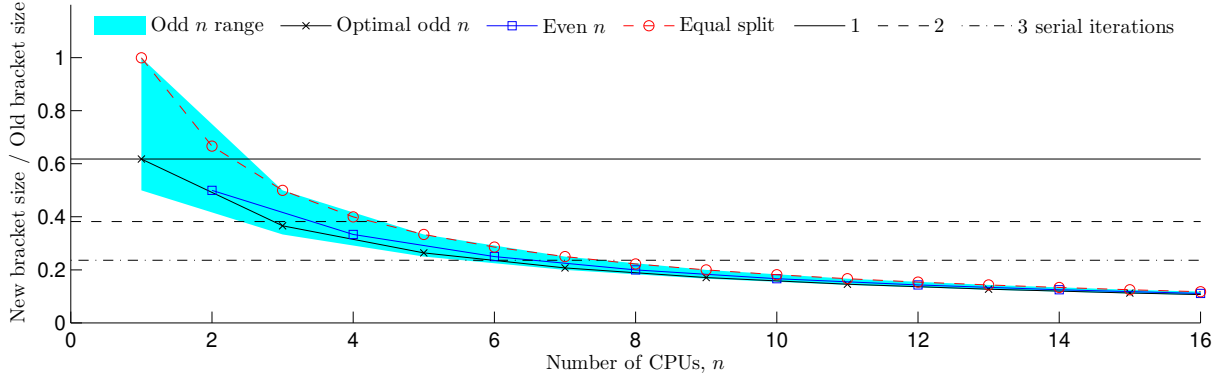


Figure 7: (Color Online) Comparison of different approaches to line minimization using the golden line search and its parallel equivalents, showing that evaluating several costs in parallel speeds up the convergence of the minimization step.

is difficult to enforce this constant aspect ratio. Furthermore, for $n > 1$, the worst case scenario ensures that the next bracket is at most of size $2l/(n+1) < l$, so the need for a constant aspect ratio is not as drastic as for $n = 1$. For simplicity, it may therefore be preferable not to attempt to enforce the constant aspect ratio condition, unless a purely parallel golden section search algorithm is used.

References

- [1] Å KERVIK, E., BRANDT, L., HENNINGSON, D. S., HÆ PFFNER, J., MARXEN, O., AND SCHLATTER, P. Steady solutions of the Navier-Stokes equations by selective frequency damping. *Phys. Fluids* 18, 6 (2006), 068102.
- [2] AHUJA, S., AND ROWLEY, C. W. Feedback control of unstable steady states of flow past a flat plate using reduced-order estimators. *J. Fluid Mech.* 645, 2010 (Feb. 2010), 447.
- [3] ANDERSON, E. A., AND SZEWCZYK, A. A. Effects of a splitter plate on the near wake of a circular cylinder in 2 and 3-dimensional flow configurations. *Exp. Fluids* 23 (June 1997), 161–174.
- [4] BERGMANN, M., AND CORDIER, L. Optimal control of the cylinder wake in the laminar regime by trust-region methods and POD reduced-order models. *J. Comput. Phys.* 227, 16 (Aug. 2008), 7813–7840.
- [5] BERGMANN, M., CORDIER, L., AND BRANCHER, J.-P. Optimal rotary control of the cylinder wake using proper orthogonal decomposition reduced-order model. *Phys. Fluids* 17, 9 (2005), 097101.
- [6] BERGMANN, M., CORDIER, L., AND BRANCHER, J.-P. On the generation of a reverse von Karman street for the controlled cylinder wake in the laminar regime. *Phys. Fluids* 18, 2 (2006), 028101.
- [7] BERGMANN, M., CORDIER, L., AND BRANCHER, J.-P. On the power required to control the circular cylinder wake by rotary oscillations. *Phys. Fluids* 18, 8 (2006), 088103.
- [8] BEWLEY, T. R., MOIN, P., AND TEMAM, R. DNS-based predictive control of turbulence: an optimal benchmark for feedback algorithms. *J. Fluid Mech.* 447 (Oct. 2001), 179–225.
- [9] BRAZA, M., CHASSAING, P., AND MINH, H. Numerical study and physical analysis of the pressure and velocity fields in the near wake of a circular cylinder. *J. Fluid Mech.* 165 (1986), 79–130.
- [10] CHOI, H., JEON, W.-P., AND KIM, J. Control of Flow Over a Bluff Body. *Annu. Rev. Fluid Mech.* 40, 1 (Jan. 2008), 113–139.
- [11] CHOI, S., CHOI, H., AND KANG, S. Characteristics of flow over a rotationally oscillating cylinder at low Reynolds number. *Phys. Fluids* 14, 8 (2002), 2767.

[12] COLONIUS, T., AND TAIRA, K. A fast immersed boundary method using a nullspace approach and multi-domain far-field boundary conditions. *Comput. Method Appl. M.* 197, 25–28 (Apr. 2008), 2131–2146.

[13] DOWLING, A. P., AND MORGANS, A. S. Feedback Control of Combustion Oscillations. *Annu. Rev. Fluid Mech.* 37, 1 (Jan. 2005), 151–182.

[14] GRIFFIN, O. M., AND HALL, S. M. Vortex Shedding Lock-on and Flow Control in Bluff Body. *J. Appl. Mech. -T. ASME* 113 (1991).

[15] HE, J.-W., GLOWINSKI, R., METCALFE, R., NORDLANDER, A., AND PERIAUX, J. Active Control and Drag Optimization for Flow Past a Circular Cylinder. *J. Comput. Phys.* 163, 1 (Sept. 2000), 83–117.

[16] HENDERSON, R. D. Nonlinear dynamics and pattern formation in turbulent wake transition. *J. Fluid Mech.* 352 (1997), 65–112.

[17] HOMESCU, C., NAVON, I. M., AND LI, Z. Suppression of vortex shedding for flow around a circular cylinder using optimal control. *Int. J. Numer. Methods Fluids* 69, March 2001 (2002), 43–69.

[18] HUERRE, P., AND MONKEWITZ, P. A. Local and Global Instabilities in Spatially Developing Flows. *Annu. Rev. Fluid Mech.*, 22 (1990), 473–537.

[19] JOE, W. T., COLONIUS, T., AND MACMYNOWSKI, D. G. Optimized Waveforms for Feedback Control of Vortex Shedding. In *Active Flow Control II* (Berlin, Germany, 2010), R. King, Ed., Springer, pp. 391–404.

[20] JORDI, B. E., COTTER, C. J., AND SHERWIN, S. J. Encapsulated formulation of the selective frequency damping method. *Phys. Fluids* 26, 3 (Mar. 2014), 034101.

[21] KANG, S., CHOI, H., AND LEE, S. Laminar flow past a rotating circular cylinder. *Phys. Fluids* 11, 11 (1999), 3312.

[22] LAUGA, E., AND BEWLEY, T. R. The decay of stabilizability with Reynolds number in a linear model of spatially developing flows. *P. Roy. Soc. A. - Math. Phys.* 459, 2036 (Aug. 2003), 2077–2095.

[23] LI, Z., NAVON, I. M., HUSSAINI, M. Y., AND LE DIMET, F.-X. Optimal control of cylinder wakes via suction and blowing. *Comput. Fluids* 32 (2003), 149–171.

[24] LU, L., QIN, J.-M., TENG, B., AND LI, Y.-C. Numerical investigations of lift suppression by feedback rotary oscillation of circular cylinder at low Reynolds number. *Phys. Fluids* 23, 3 (2011), 033601.

[25] MIN, C., AND CHOI, H. Suboptimal feedback control of vortex shedding at low Reynolds numbers. *J. Fluid Mech.* 401 (Dec. 1999), 123–156.

[26] PARK, J., KWON, K., AND CHOI, H. Numerical solutions of flow past a circular cylinder at Reynolds numbers up to 160. *KSME Int. J.* 12, 6 (1998), 1200–1205.

[27] PRESS, W. H., TEUKOLSKY, S. A., VETTERLING, W. T., AND FLANNERY, B. P. *Numerical Recipes in Fortran The Art of Scientific Computing*, third ed. Cambridge University Press, Cambridge, 2007.

[28] PROTAS, B., AND STYCZEK, A. Optimal rotary control of the cylinder wake in the laminar regime. *Phys. Fluids* 14, 7 (2002), 2073.

[29] PROTAS, B., AND WESFREID, J.-E. Drag force in the open-loop control of the cylinder wake in the laminar regime. *Phys. Fluids* 14, 2 (2002), 810.

[30] PROVANSAL, M., MATHIS, C., AND BOYER, L. Bénard-von Karman instability : transient and forced regimes. *J. Fluid Mech.* 182 (1987), 1–22.

[31] SCHUMM, M., BERGER, E., AND MONKEWITZ, P. A. Self-excited oscillations in the wake of two-dimensional bluff bodies and their control. *J. Fluid Mech.* 271 (1994).

- [32] SHIELS, D., AND LEONARD, A. Investigation of a drag reduction on a circular cylinder in rotary oscillation. *J. Fluid Mech.* 431 (Mar. 2001), 297–322.
- [33] SIEGEL, S. G., COHEN, K., AND McLAUGHLIN, T. Numerical Simulations of a Feedback-Controlled Circular Cylinder Wake. *AIAA J.* 44, 6 (June 2006), 1266–1276.
- [34] STRYKOWSKI, P. J., AND SREENIVASAN, K. R. On the formation and suppression of vortex 'shedding' at low Reynolds numbers. *J. Fluid Mech.* 218 (1990), 71–107.
- [35] TAIRA, K., AND COLONIUS, T. The immersed boundary method: A projection approach. *J. Comput. Phys.* 225, 2 (Aug. 2007), 2118–2137.
- [36] THIRIA, B., GOUJON-DURAND, S., AND WESFREID, J.-E. The wake of a cylinder performing rotary oscillations. *J. Fluid Mech.* 560 (July 2006), 123.
- [37] TOKUMARU, P. T., AND DIMOTAKIS, P. E. Rotary oscillation control of a cylinder wake. *J. Fluid Mech.* 224 (Apr. 1991), 77–90.
- [38] TU, J. H., AND ROWLEY, C. W. An improved algorithm for balanced POD through an analytic treatment of impulse response tails. *J. Comput. Phys.* 231, 16 (June 2012), 5317–5333.
- [39] WILLIAMSON, C. H. K. Vortex Dynamics in the Cylinder Wake. *Annu. Rev. Fluid Mech.* 28 (1996), 477–539.